Multistep Reaction Processes in Epoxide Formation from 1-Chloro-2-methyl-2-propanol on Ag(110) Revealed by TPXPS and TPD Experiments

H. Piao, K. Adib, Z. Chang, and J. Hrbek

Department of Chemistry, Brookhaven National Laboratory, Upton, New York 11973

M. Enever and Mark A. Barteau*

Department of Chemical Engineering, Center for Catalytic Science and Technology, University of Delaware, Newark, Delaware 19716

D. R. Mullins

Oak Ridge National Laboratory, PO Box 2008, MS 6201, Oak Ridge, Tennessee 37831-6201

Received: July 1, 2003; In Final Form: October 1, 2003

Synchrotron-based temperature-programmed X-ray photoelectron spectroscopy (TPXPS) in combination with temperature-programmed desorption (TPD) has been used to track C−Cl scission in the reaction of 1-chloro-2-methyl-2-propanol (Cl-*tert*-BuOH) on oxygen-containing Ag(110) surfaces. The results show that the oxygen pre-coverage strongly influences the cleavage of the C−Cl bond. At low coverages, C−Cl scission of chloro-*t*-butoxide intermediates begins at 200 K and isobutylene oxide (IBO) appears with a peak temperature of 235 K; at higher coverages, the onset of C−Cl scission is shifted upward by 50 K and the IBO peak by 80 K. Quantitative models for the surface reaction kinetics were developed from the experimental data. These show that the reaction of adsorbed intermediates does not occur by an S_N2 process that releases IBO directly into the gas phase. Instead, C−Cl scission deposits organic intermediates or products on the surface, and the appearance of IBO in the gas-phase lags the appearance of atomic chlorine on the surface. For the lower temperature channel, the rate of IBO evolution in TPD is influenced by the kinetics of both C−Cl scission and molecular IBO desorption. At higher temperatures, surface diffusion processes to open surface sites limit the rate of IBO production. Comparison with results for chlorine diffusion into silver suggests that this is the relevant diffusion process.

1. Introduction

Several recent studies have been devoted to the identification and characterization of surface oxametallacycles (cyclic structures having an −O−C−C− structure bound at both ends to the metal surface).[1−16] These species have been proposed as surface intermediates in the process of olefin epoxidation. Understanding the formation and the reactivity of these oxametallacycle intermediates on silver surfaces is a key to establishing the mechanism of epoxide formation. Synthetic routes that have permitted spectroscopic characterization of these intermediates include reactions of halohydrins[1,2,11,13,15] and ring opening of epoxides.[5,10,14] The isolation and spectroscopic identification of stable surface oxametallacycle intermediates have been recently reported for the reaction of 2-iodoethanol on Ag(110)[1,2] and Ag(111).[11,13,15] Recent examples of epoxide ring opening include the reaction of ethylene oxide (EO) on Ag(111)[10] and of 1-epoxy-3-butene (EpB) on Ag(110).[5] Both cases have demonstrated the formation of stable surface oxametallacycles and their subsequent reaction to regenerate the parent epoxides plus other products. The principal techniques employed in these previous studies have been high-resolution electron energy loss spectroscopy (HREELS) and temperature-programmed desorption (TPD).[1,2,5−11] Density functional theory (DFT) calculations have been used to identify the surface oxametallacycle intermediates on the basis of their spectroscopic signatures.[2−7,9−11]

As part of a continuing effort to improve the understanding of the reaction mechanisms of epoxide formation, we have focused on the reaction of chloro-*tert*-butyl alcohol (Cl^{t}BuOH) on oxygen-covered Ag(110) surfaces to produce isobutylene oxide (IBO). Chlorohydrins are used for the commercial noncatalytic production of some epoxides, for example, the manufacture of propylene oxide via the propylene chlorohydrin process.[17] Thus elucidation of the mechanism of epoxide formation from the reaction of chlorohydrins on silver surfaces can shed light on the similarities and differences between homogeneous and heterogeneous processes for epoxide formation. The other primary consideration for the selection of this system is that halohydrins have been proven to be useful reagents for the synthesis of surface oxametallacycles.[1,2,11,13,15] Moreover, *tert*-butyl alcohol has been shown to react on oxygen-covered Ag(110) to form IBO; this reaction was suggested to proceed through an oxametallacycle intermediate.[18] It has been shown that Cl^{t}BuOH reacts in an analogous fashion on the oxygen-covered surface to produce chloro-*tert*-butoxy (Cl^{t}BuO-(ad)) intermediates and water. Cl^{t}BuO(ad) then reacts via C−Cl bond cleavage to produce IBO, depositing surface chlorine atoms.[8] Our previous report also suggested that the IBO formation may proceed through a surface oxametallacycle

* Corresponding author. Tel: 1-302-831-8905; fax: 1-302-831-8201; e-mail address: barteau@che.udel.edu.

10.1021/jp035892e CCC: $25.00
Published on Web 11/22/2003

SCHEME 1

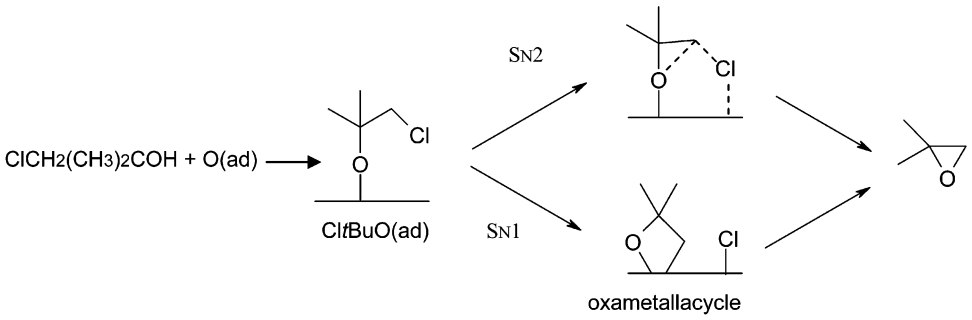

intermediate. As will be shown below, C−Cl bond cleavage is one of the key steps to produce IBO. However, the C−Cl bond cleavage mechanism has not been fully understood. This motivated the study of the surface reaction to determine whether the surface chlorohydrin reaction follows an S_N1 mechanism in which cleavage of the C−Cl bond and IBO formation occur in a stepwise manner or a concerted S_N2 path, as illustrated in Scheme 1.

In our previous paper,[8] laboratory-based XPS experiments were performed to study this reaction. In combination with the TPD results, stepwise XPS spectra showed that the C−Cl bond cleavage roughly coincided with IBO desorption, implying that the reaction mechanism might best be described as S_N2. Unfortunately, the results were not conclusive because of the difficulty of locating the narrow temperature range, if any exists, in which C−Cl bond cleavage occurs before IBO formation/desorption begins. Recent work has highlighted the power of synchrotron-based XPS for real time study of surface reactions.[19] In the present study, we have utilized temperature-programmed XPS (TPXPS) experiments to perform transient studies of the C−Cl bond cleavage mechanism. Our previous XPS results also indicated that the laboratory-based XPS spectra suffer from significant resolution problems that obscure important spectral information. Thus, higher resolution spectra are an additional advantage of the synchrotron-based studies. The improvement in signal-to-noise ratio achieved because of the greater intensity of the synchrotron-radiation beam can also facilitate studies at low adsorbate coverages. The tunability of the photon energy allows the tuning of photoelectron cross-sections to achieve optimal elemental sensitivities.

In this paper, temperature-programmed XPS (TPXPS) based on Cl2p and C1s lines has been used to study the kinetics of C−Cl scission. The C−Cl bond cleavage begins at 200 and 250 K on low (0.1 monolayer (ML)) and high O-covered (0.3 ML) surfaces, respectively. In neither case is the kinetics of C−Cl scission alone sufficient to account for the rate of IBO production. Quantitative analysis and comparison of the TPXPS and TPD results provide insights into the additional surface processes that influence the rate of epoxide evolution.

2. Experimental Section

Soft X-ray photoelectron spectroscopy (XPS) experiments were performed in a UHV chamber on the U12A beamline at the Brookhaven National Laboratory. The chamber was pumped by a combination of turbomolecular and cryopumps resulting in a base pressure less than 4×10^{-10} Torr. The chamber was also equipped with a mass spectrometer for TPD experiments, an ion gun, a pinhole doser, and a leak valve. The XPS spectra were collected in the fixed-pass energy mode using a concentric hemispherical analyzer. Energy calibration was performed individually for every spectrum by aligning the energy scale to the Fermi edge. A $Ag3d_{5/2}$ peak position of 368.2 eV was derived from independent calibrations to the Fermi edge of a clean Ag(110) single crystal. The use of synchrotron radiation has resulted in major improvements in spectral resolution. Using two sets of gratings as well as various photon energies, energy resolution better than 0.1 eV can be obtained.

Temperature-programmed XPS (TPXPS) data were collected using a linear heating rate of 1 K s^{-1}. Identification of the desorbed products in TPD experiments was carried out by deconvolution of the contributions of mass fragments from each product. The mass fragmentation pattern for each product was determined experimentally by backfilling the chamber with the pure component and collecting mass spectra of the stable fragment ions. The TPD data were collected using the same heating rate (1 K s^{-1}) as in TPXPS experiments.

The Ag(110) single-crystal disk, ca. 12.5 mm diameter × 2 mm thick, was mounted on a 0.25-mm Ta wire loop which was spot welded to two additional Ta wires used for resistive heating and suspended from the bottom of a liquid nitrogen reservoir. The sample could be resistively heated to >900 K or cooled to 110 K. The sample temperature was monitored by a K-type thermocouple spot welded to the Ta wire loop at the bottom of the sample. The sample was cleaned by successive cycles of Ar^+ ion bombardment at 300 K followed by annealing at 900 K. Surface cleanliness was confirmed by the absence of O1s and C1s signals in the XPS spectrum as well as by oxygen TPD. 1-Chloro-2-methyl-2-propanol (Cl^{t}BuOH, Aldrich, 97%) was stored in a glass-dosing tube attached to the main chamber through a leak valve. It was purified by repeated freeze−pump−thaw cycles. For both XPS and TPD measurements, the surface was pre-covered at 300 K with different coverages of oxygen, subsequently cooled to 110 K, and dosed with a multilayer coverage of Cl^{t}BuOH. The introduction of O_2 to the surface was accomplished by direct dosing through the pinhole doser which was mounted in the UHV chamber. Dosing of Cl^{t}BuOH was accomplished by backfilling the UHV chamber with Cl^t-BuOH through a leak valve and monitoring the dosing time at a given pressure.

3. Results

3.1. Isobutylene Oxide Formation via C−Cl Bond Cleavage. For all of the following studies, prior to Cl^{t}BuOH exposure the Ag(110) surface was pre-covered at 300 K with atomic oxygen. Surface oxygen is required to initiate reactions of many alcohols on silver surfaces, since surface oxygen facilitates the abstraction of the hydroxyl proton of the alcohol, resulting in the formation of surface alkoxide species.[18,20−22] We have previously conducted TPD studies of the thermal chemistry of Cl^{t}BuOH on clean Ag(110) in a separate UHV system.[8] Those results indicated that Cl^{t}BuOH does not react on clean Ag(110) but does react on the O-covered surface to form IBO. To ensure

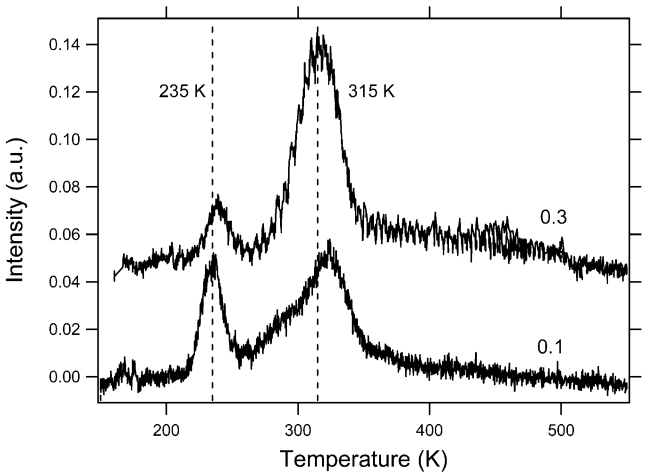

Figure 1. Temperature-programmed desorption spectra of IBO (*m*/*e* = 41) product for two different oxygen pre-coverages (0.1 and 0.3 monolayers (ML)).

consistency between TPD peak temperatures on the two UHV systems, TPD experiments examining IBO production from Cl^t-BuOH on O-covered Ag(110) were also performed in the UHV system attached to the U12A beamline. Figure 1 shows desorption spectra of IBO (monitoring the fragment with *m*/*e* = 41) from the reaction of Cl^{t}BuOH at two oxygen atom pre-coverages (0.1 and 0.3 ML). The IBO product spectra exhibit two desorption features at 235 and 315 K, which are comparable to the values of 230 and 305 K in the previous study. Low initial oxygen coverages favor IBO production via the 235 K channel, while larger coverages promote the desorption of IBO near 315 K. In addition, upon increasing the initial oxygen coverage, the low-temperature peak shifted slightly to higher temperatures. According to the previous TPD results for IBO production across a wide range of oxygen pre-coverages (0.021−0.30 ML),[8] the 235 K feature appears first at very low oxygen exposures and the intensity of this feature becomes relatively constant at higher oxygen coverages. As the oxygen pre-coverage is increased, the dominant feature in the IBO desorption spectrum is the peak at 315 K. For the low oxygen pre-covered surface in Figure 1, a prominent shoulder was apparent at the low-temperature side (260−300 K) of the 315 K desorption state. This feature is evident from the lowest oxygen exposures.[8] An increase of the initial oxygen coverage leads to the disappearance of this feature and to the enhancement of the peak at 315 K. In addition, this shoulder (260−300 K) matches the temperature window for Cl^t-BuOH desorption (not shown, see ref 8). The small Cl^{t}BuOH desorption channel in this region may be associated with recombination of a small amount of Cl^{t}BuO(ad) with atomic hydrogen to form molecular Cl^{t}BuOH. All the data indicate that the oxygen pre-coverage has a strong effect on IBO formation. This may be related to the variation of the surface chemistry caused by the combined effects of oxygen-induced surface reconstruction and surface crowding. This will be discussed in greater detail below. In this work, the oxygen coverage was estimated by comparing the relative peak areas of these two desorption states to our previous TPD results at known oxygen coverages. The corrected peak area for oxygen desorption from a Ag(110) surface covered with 0.33 ML of oxygen atoms was used as a standard reference.[8] A coverage of 0.33 ML corresponds to a p(3 × 1) oxygen-covered surface observed by LEED. In this study, two different oxygen coverages of 0.1 and 0.3 ML were used for Cl^{t}BuOH reaction studies. Complete titration of surface oxygen atoms with alcohols to form water should yield two alkoxides per oxygen atom initially adsorbed.

While our previous report[8] detailed desorption studies of Cl^t-BuOH and IBO, the primary focus of this work is on the high-resolution XPS investigations of C−Cl bond scission. The samples were characterized by the core level Ag3d spectra of the substrate and C1s and Cl2p spectra of the organic adlayer. In this paper, we focus on the Cl2p and C1s core levels of the organic adsorbates. Figure 2 shows a comparison of a series of representative Cl2p spectra collected using both laboratory- and synchrotron-based X-ray sources. The laboratory-based XPS spectra[8] were collected using a Mg Kα source in a separate UHV chamber that has been described previously.[23,24] As can be seen, because of the high resolution of the synchrotron data, the spin−orbit splitting of the Cl2p line is clearly observed, that is, each Cl-containing species gives rise to two lines ($Cl2p_{3/2}$ and $Cl2p_{1/2}$); the $Cl2p_{3/2}$:$Cl2p_{1/2}$ intensity ratio is 2:1 and the energy separation is 1.6 eV. In addition, the feature corresponding to chemisorbed atomic Cl at a binding energy of 198.1 eV ($Cl2p_{3/2}$) has been clearly resolved. These changes are not apparent in the spectra obtained via laboratory-based XPS: the $2p_{1/2}$ component of the atomic chlorine produced by the reaction overlaps with the $2p_{3/2}$ component of the adsorbed organic Cl species. The resolution enhancement leads to an improvement in photoelectron line widths (fwhm) compared to those for Mg Kα radiation: ∼1 eV compared to ∼2 eV.

Figure 3 shows the evolution of the synchrotron-based Cl2p spectrum following annealing to incrementally higher temperatures (as indicated) for the surfaces on which Cl^{t}BuOH was reacted with oxygen pre-coverages of 0.3 (Figure 3a) and 0.1 ML (Figure 3b). For both high and low initial oxygen coverages, the surface upon dosing Cl^{t}BuOH at 110 K (the uppermost spectrum) is dominated by a single, well-resolved Cl2p doublet structure and is characterized by only organic chlorine species. The adsorption of Cl^{t}BuOH at 110 K following an oxygen pre-coverage of 0.3 ML gives rise to $Cl2p_{3/2}$ and $2p_{1/2}$ lines centered at 202.2 and 200.6 eV, respectively (see Figure 3a). These characteristic features have been unambiguously attributed to the C−Cl bond present in the chemisorbed layer of Cl^{t}BuOH and Cl^{t}BuO(ad).[8] In the spectra as shown in Figure 3b for 0.1 ML oxygen coverage, however, the doublet structure of Cl2p at 110 K is relatively broader than that for the higher oxygen coverage; the peak positions are also shifted to higher binding energy by approximately 0.2 eV compared to those for higher oxygen pre-coverages. Heating causes the peaks for the lower oxygen pre-coverage in Figure 3b to shift to lower binding energy. However, there is no pronounced intensity change after the initial brief heating to 150 K or even higher temperature, indicating that this shift may not be due to the desorption of significant amounts of molecular Cl^{t}BuOH. This shift may be due to differences in the surface binding configuration between physisorbed and chemisorbed Cl^{t}BuOH or relaxation shifts of the type described for other molecules such as methyl thiolate on Ni(111)[25] and octane on Cu (100).[26] It is also possible that the titration of oxygen atoms to form water is not completed until the surface layer is heated; the small binding energy shift observed may represent completion of the reaction of Cl^{t}BuOH to form the corresponding alkoxides. Our previous study demonstrated that for the oxygen pre-coverages utilized in the present work (0.1−0.3 ML), desorption of molecular Cl^{t}BuOH from the low-temperature (185 K) state observed on the clean Ag(110) surface is suppressed.

With increasing surface temperature, the doublet structure of the Cl2p lines becomes sharper for both coverages. Spectra at 150−200 K in Figure 3a and b are clearly dominated by chemisorbed chloro-*tert*-butoxide species. Chlorine is deposited

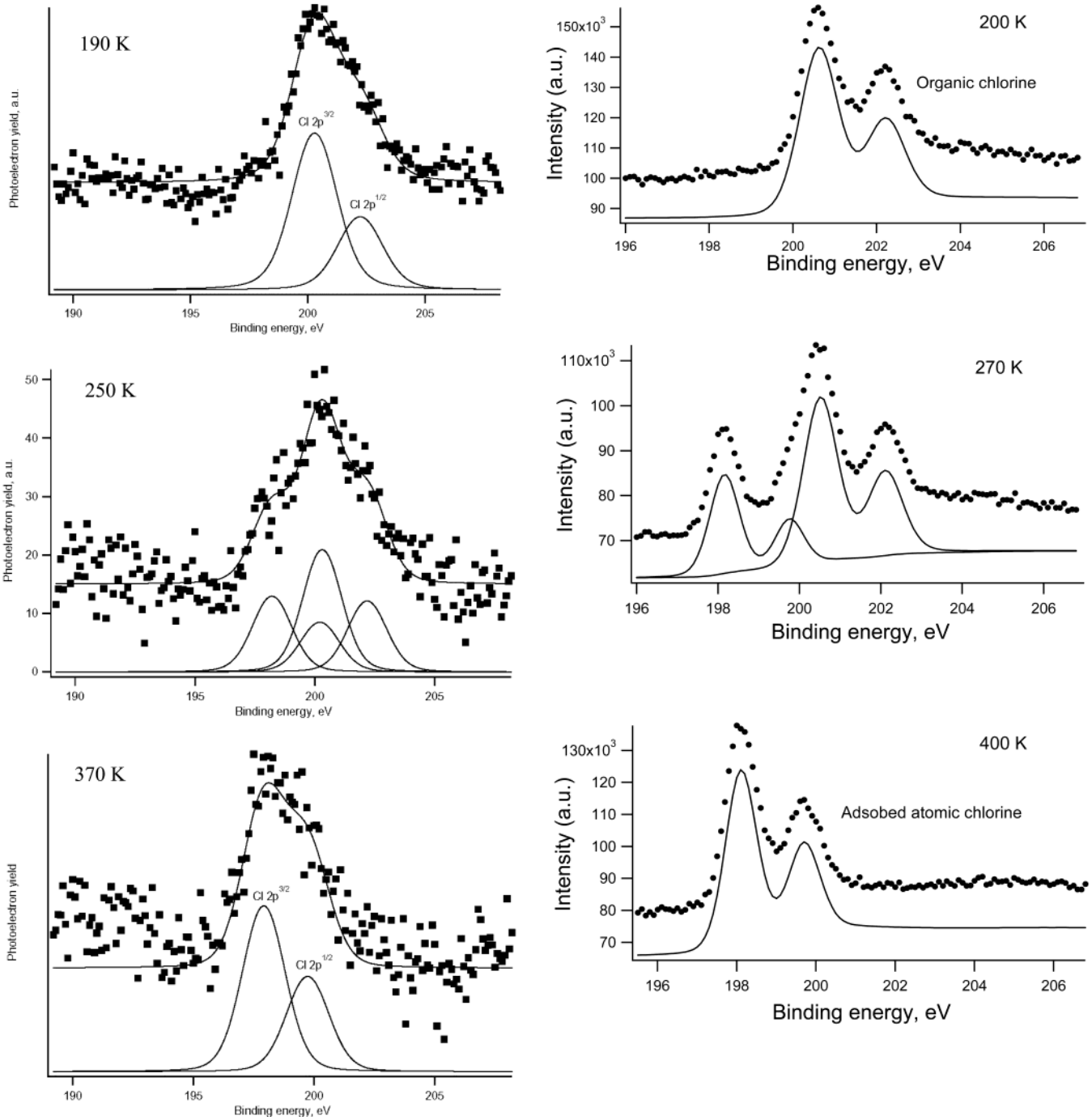

Figure 2. Comparison of a series of representative Cl2p spectra collected using (a) laboratory-[8] and (b) synchrotron-based X-ray sources. The surface was pre-covered at 300 K with 0.3 ML oxygen and cooled to 110 K for a multilayer dose of Cl^{t}BuOH. The surface was then heated at the same rate as in TPD experiments to the temperature of interest, then cooled rapidly for XPS analysis.

on the surface by reaction of chloro-*tert*-butoxides, as is shown by the appearance of a new feature at a binding energy of 198.1 eV. This feature is first apparent at 250 K in the spectra of Figure 3a and at 200 K in Figure 3b. By 300−400 K the Cl^t-BuO(ad) is completely decomposed, and the Cl 2p peaks of chemisorbed atomic Cl can be clearly resolved, with spin−orbit $2p_{3/2}$ and $2p_{1/2}$ features located at 198.1 and 199.7 eV, respectively. These values are in good agreement with those associated with a silver chloride species.[8] The spectra obtained at intermediate temperatures (200−300 K) in Figure 3 demonstrate the reaction of chloro-*tert*-butoxide species to deposit atomic Cl on the surface; the Cl peaks of the organic species are progressively supplanted by those of Ag−Cl species. For both oxygen pre-coverages, C−Cl bond cleavage is almost complete after annealing the surface to 300 K. Upon heating to 900 K, surface Cl is completely removed. This is consistent with results reported by Bowker et al.[27] who observed desorption of Cl in the form of AgCl after annealing to temperatures near 900 K.

Figure 4 shows the evolution of the corresponding C1s spectra as a function of annealing temperature. For the 0.3 ML oxygen pre-coverage (Figure 4a), two main features are well resolved. The first feature at 285.1 eV arises from contributions associated with the two methyl groups of the chloro-*tert*-butoxide intermediate. The second feature at 286.6 eV is assigned to the two carbons of the chloro-*tert*-butoxide attached to electronegative substituents, that is, oxygen and chlorine. It is well established that the presence of one oxygen or one chlorine atom on a

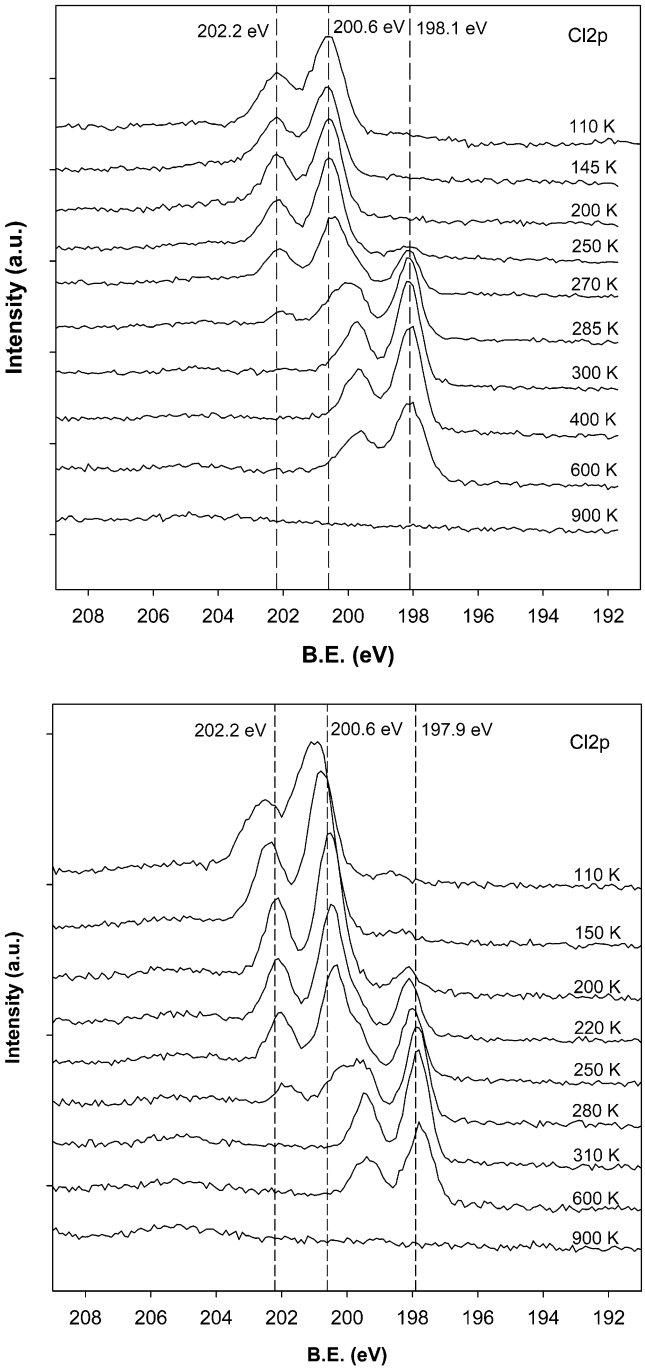

Figure 3. The evolution of Cl2p spectra after heating to different temperatures for a saturation exposure of Cl^{t}BuOH. (a, upper panel) 0.3 ML and (b, lower panel) 0.1 ML oxygen atom pre-coverage.

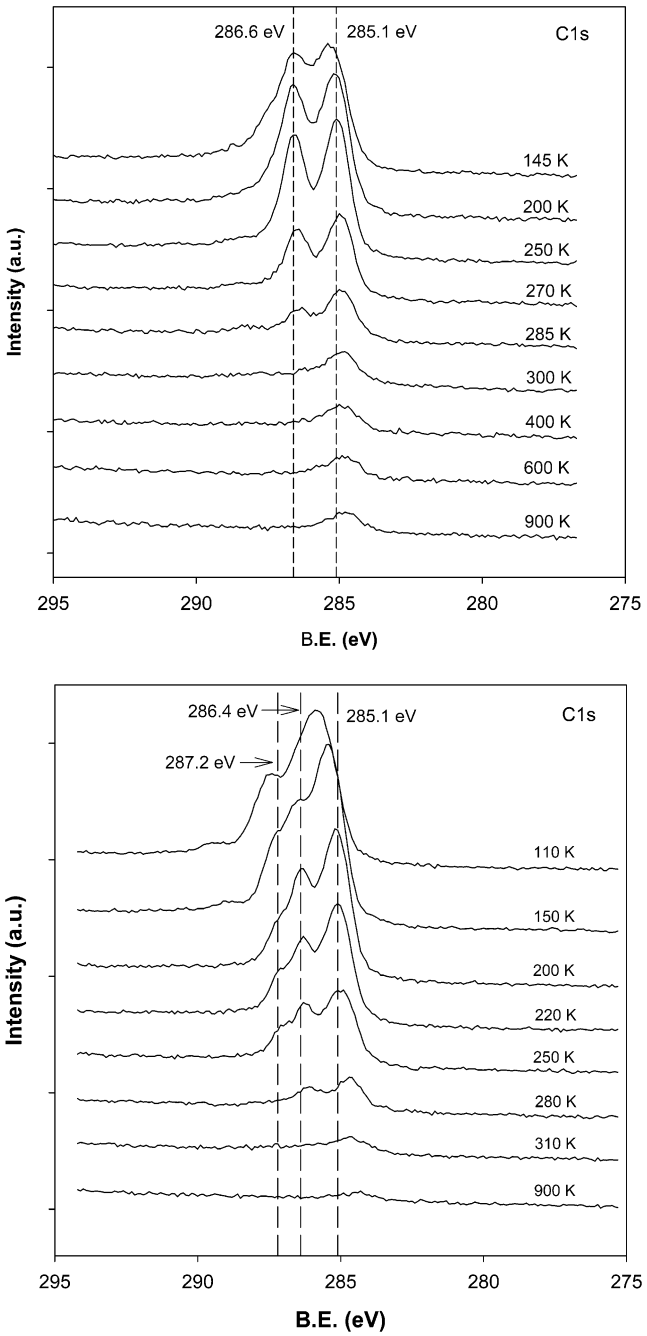

Figure 4. The evolution of C1s spectra after heating to different temperatures for a saturation exposure of Cl^{t}BuOH. (a, upper panel) 0.3 ML and (b, lower panel) 0.1 ML oxygen atom pre-coverage.

carbon atom chemically shifts its binding energy by about 1.3 to 1.4 eV.[28] The roughly equal magnitudes of the peaks at 285.1 and 286.6 eV support this assignment. Figure 4b represents the C1s spectra for the 0.1 ML oxygen pre-coverage; it should not be surprising that the C1s line structure below 150 K exhibits some degree of broadening as well as shifts toward higher binding energies, consistent with the observations for Cl2p spectra, as discussed above. The main features at 285.1 and 286.4 eV clearly match those in Figure 4a. However, the relative intensity ratio of these two features becomes distorted from that for the high oxygen pre-covered surface, and a shoulder develops at ca. 287.2 eV, which was not apparent for the high oxygen pre-covered surface. These changes of the spectral shape are evidence for the existence of more than one chemically inequivalent form of carbon species. As is also shown in Figure 4, the increase of the surface temperature results in decreases of the intensities for all the peaks. This is indicative of the desorption of Cl^{t}BuOH and reaction of Cl^{t}BuO(ad) to form volatile products. In addition, the peak positions of all the peaks shifted slightly to lower binding energy with increasing surface temperature. This effect may be due to the steric or electronic effects encountered at relatively higher coverages of chlorine and coadsorbed organic species such as Cl^{t}BuO during the reaction. Following annealing of the surface to a temperature as high as 900 K, the spectra indicate traces of residual carbon species with C1s peak position close to the value for graphite at 284.4 $\pm$ 0.2 eV.[29−31]

The C1s spectral components have been resolved by performing a detailed peak-fitting analysis of the spectra. Figure 5 shows

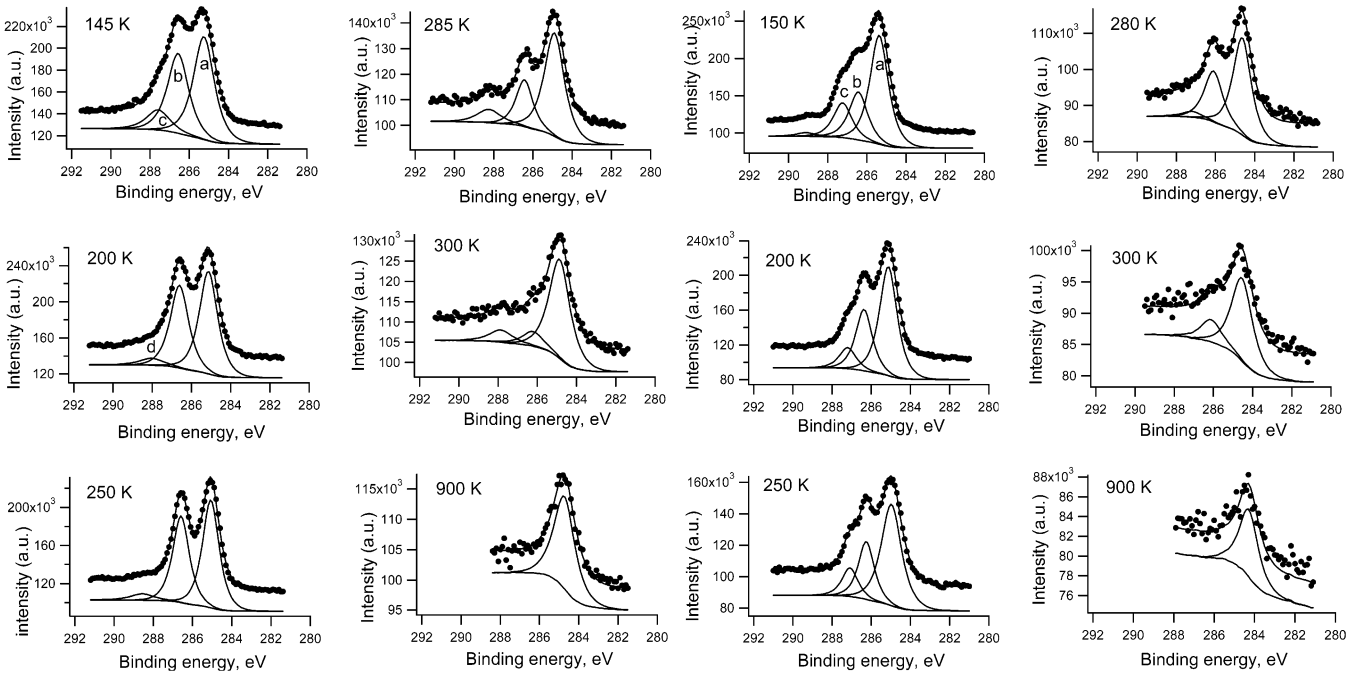

Figure 5. A series of peak-fitted C1s spectra obtained after heating to different temperatures for a saturation exposure of Cl^{t}BuOH. (a, left panels) 0.3 ML and (b, right panels) 0.1 ML oxygen atom pre-coverage.

representative spectra together with the results of the peak-fitting analysis for both low and high oxygen pre-covered surfaces. For the low oxygen pre-covered surface (Figure 5b), the fitting results of the spectrum at 150 K revealed the existence of two minor components, with C1s binding energies at 287.2 ± 0.2 and 289.1 ± 0.2 eV, respectively. The trace feature at 289.1 eV is at a binding energy more typical of carboxylic acids than alcohols and may represent a minor impurity. In any case it disappears by 200 K. The other new feature is resolved at the binding energy of 287.2 ± 0.2 eV, which is 2.0 eV higher than that for the methyl groups. Increasing the surface temperature results in a slight decrease of this contribution and it almost disappears after annealing the surface to approximately 280 K. This feature likely represents small amounts of adsorbed molecular species, either the Cl^{t}BuOH reactant or possibly reaction products. Spectra obtained following reaction of Cl^t-BuOH with the 0.3 ML oxygen pre-covered surface also show evidence for an additional peak in the same energy range, but this peak is much less prominent on the more densely covered surface.

The results of this and our previous study[8] demonstrate that variation of the oxygen pre-coverage influences the surface chemistry of Cl^{t}BuOH on Ag(110). Titration of 0.3 ML of oxygen atoms to completion would produce 0.6 ML of bulky Cl^{t}BuO intermediates, resulting in a very crowded surface. Even the density of Cl^{t}BuO species produced by titration of 0.1 ML of oxygen atoms is sufficient to block the adsorption of much additional Cl^{t}BuOH, as noted above. Thus, it is not surprising that significant coverage effects are observed in the reaction of Cl^{t}BuO intermediates, particularly since this reaction deposits a nonvolatile product, Cl atoms (which will also tie up surface sites), in addition to the IBO product which desorbs.

To gain more understanding of the C−Cl bond scission process and to determine precisely the temperature range in which it occurs, Temperature-programmed XPS (TPXPS) experiments were performed by tracking the changes of the intensities of the Cl2p$_{3/2}$ signals for both Cl^{t}BuOH and Cl^{t}BuO-(ad) (200.6 ± 0.1 eV) and silver chloride (198.1 ± 0.1 eV) species as functions of annealing temperature. On the high

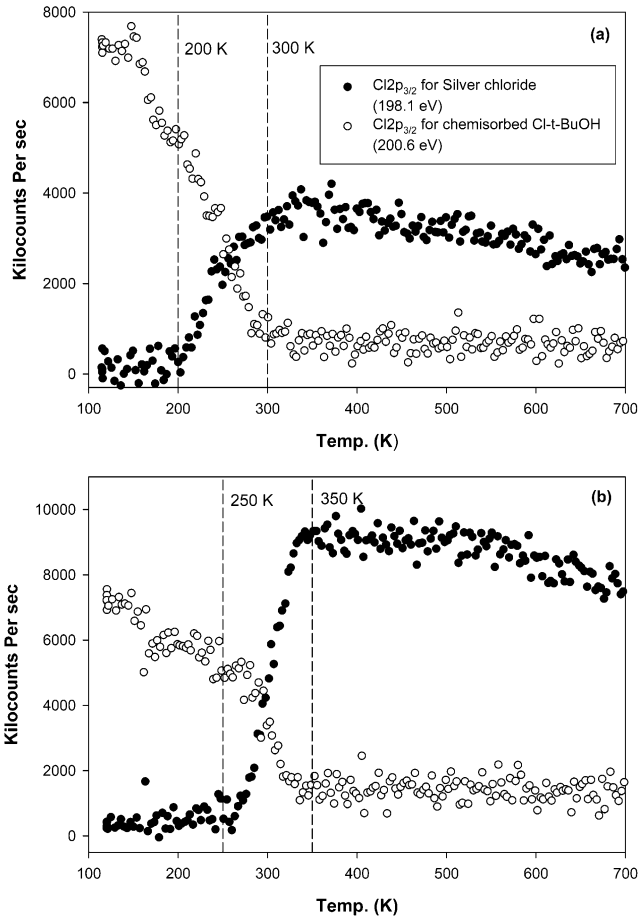

Figure 6. TPXPS results for Cl2p$_{3/2}$ lines for chemisorbed Cl^{t}BuOH and silver chloride species as a function of annealing temperatures (a) 0.1 ML and (b) 0.3 ML oxygen atom pre-coverage.

coverage surface (Figure 6b), there is a small decrease in the organic chlorine signal below 200 K, possibly reflecting the desorption of small amounts of molecularly adsorbed reactant. The decrease on the low coverage surface (Figure 6a) appears

to be more substantial, but likely reflects the shift of the entire Cl2p envelope to lower binding energy with the removal of the alcohol (See Figure 3b). As shown in Figure 3, the surface at 200 K is dominated by chloro-*tert*-butoxide species; little Cl has yet been deposited on the surface by 200 K in the transient experiments illustrated in Figure 6. Above 200 K, the $Cl2p_{3/2}$ signal for silver chloride starts to increase on the low coverage surface, reflecting the cleavage of the C−Cl bond and the formation of Ag−Cl bonds. The process of C−Cl bond cleavage and Ag−Cl bond formation is completed when the surface temperature reaches approximately 300 K. For the high O-covered surface (Figure 6b), the temperature range for the cleavage of the C−Cl bond in the TPXPS experiments exhibits a shift of approximately 50 K to higher temperatures, starting at 250 K and ending at 350 K.

3.2. Effects of Oxygen Pre-Coverage on C−Cl Bond Cleavage. As noted above, the oxygen pre-coverage (and thus the Cl^{t}BuO coverage produced) strongly influences the cleavage of the C−Cl bond. For both oxygen pre-coverages, C−Cl bond cleavage occurs at a lower temperature range (200−300 K and 250−350 K for low and high O-covered surfaces, respectively) than C−H bond cleavage at 440−510 K in *tert*-butoxy (^{t}BuO-(ad)),[18] which is consistent with the difference in C−H and C−Cl bond strengths. The TPXPS results are consistent with the TPD and XPS experiments in Figures 1 and 3, respectively, which demonstrate that on the low coverage surface the 235 K reaction channel is favored; on the higher coverage surface the 315 K channel is dominant.

A careful examination of the intensity variation of the $Cl2p_{3/2}$ signals associated with the silver chloride species in Figure 6a reveals that the C−Cl bond cleavage for the low oxygen pre-covered surface occurs in two stages: initially, the intensity increases dramatically up to 250 K; then it continues to increase more slowly up to 350 K. This is consistent with the comparable magnitudes of the 235 and 315 K IBO peaks for this system as shown in Figure 1—the contributions of each to Cl deposition are distinguishable in the TPXPS experiments. Conversely, little IBO is produced via the 235 K channel on the high coverage surface, and the TPXPS results show little deposition of atomic chlorine on this surface below 260 K.

3.3. TPXPS and TPD Simulation Results. With the refined data provided by synchrotron TPXPS and TPD experiments, modeling of potential reaction sequences was utilized to further elucidate the surface reaction chemistry. To form IBO, the C−Cl bond of the Cl^{t}BuO(ad) intermediate must be broken, producing surface-bound chlorine atoms. The TPXPS spectrum corresponding to the formation of surface chlorine was analyzed to obtain kinetic parameters for C−Cl bond scission. The low-temperature reaction channel prominent for the reaction of Cl^t-BuOH on a surface initially containing 0.1 ML O atoms was analyzed first. Since, as shown in the spectrum in Figure 1, no more than half of the volatile products were associated with the low-temperature reaction channel at this coverage, only the first half of the rise of the Cl signal in Figure 7 was utilized. The best fit is shown in Figure 7a for an activation energy of 9.5 kcal/mol and a preexponential factor of 1.2×10^8 s^{-1}. Acceptable fits could be obtained for activation energies of 7.5−12.5 kcal/mol with corresponding first-order preexponentials between 10^6 and 10^{11} s^{-1}. However, no set of parameters consistent with the TPXPS results could generate the observed IBO desorption peak at 235 K, assuming the Cl(ad) and IBO-(g) are produced by a common elementary step. The attempt to simulate the IBO TPD spectrum using the first-order rate parameters obtained from fitting the TPXPS data is shown in Figure 7b. The desorption of IBO clearly lags the C−Cl scission process. This indicates that C−Cl scission of the Cl^{t}BuO species generates an organic intermediate or product on the surface whose reaction or desorption kinetics must also be accounted for. By including a second step in the model one can simulate the observed TPD spectrum, as shown in Figure 8. Using the best-fit parameters from the TPXPS for the first step, the TPD data were best modeled by a second step with an activation energy of 13 kcal/mol and preexponential factor of $10^{11.5}$ s^{-1}. The "normal" preexponential suggests that the second step may simply be desorption of molecularly adsorbed IBO formed by the initial C−Cl scission. Comparison with available kinetic

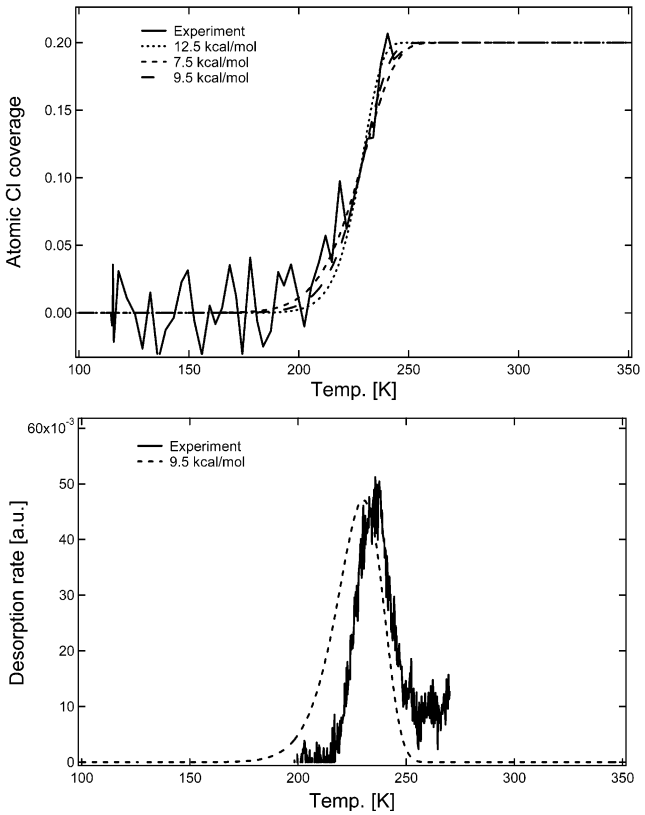

Figure 7. (a) Fit of first-order kinetics to TPXPS results for Cl atom deposition on the low oxygen atom coverage (0.1 ML) surface, and (b) comparison of predicted vs measured TPD spectra for IBO production for these kinetics.

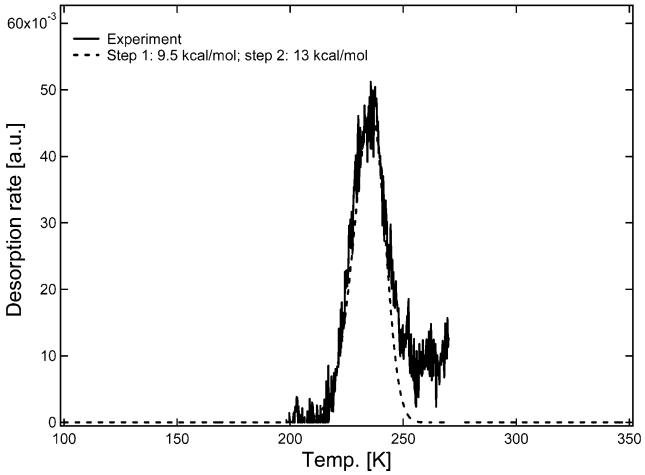

Figure 8. Match of predicted and measured TPD results at low oxygen atom coverage (0.1 ML) for a two-step model, using kinetic parameters for the first step obtained from TPXPS.

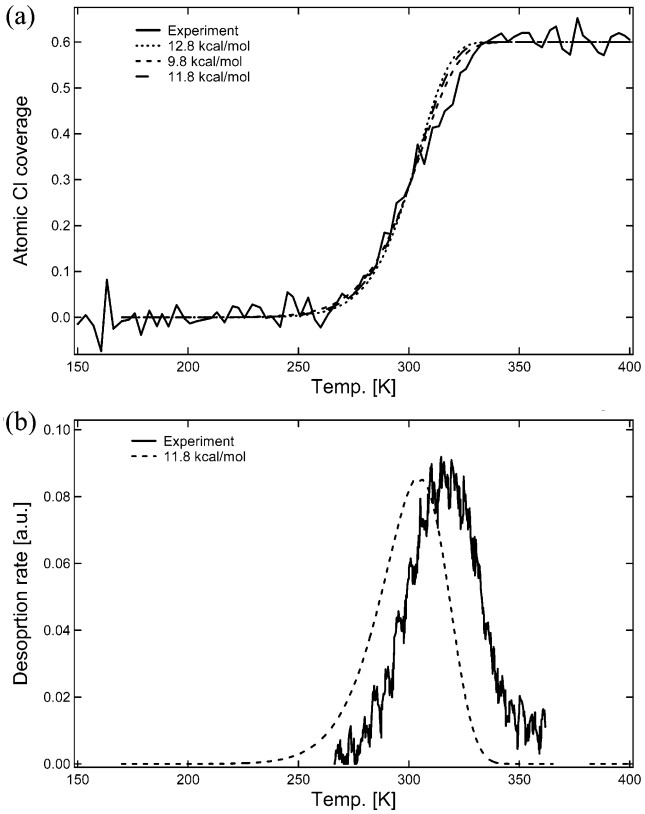

Figure 9. (a) Fit of first-order kinetics to TPXPS results for Cl atom deposition on the high oxygen atom coverage (0.3 ML) surface, and (b) comparison of predicted vs measured TPD results for IBO production for these kinetics.

parameters for desorption of C_4-epoxides from Ag(110) surfaces supports this conclusion. For example, after adsorption at low temperature, epoxybutene and butylene oxide both desorbed at 215 K.[9] These peaks were modeled with an activation energy of 14 kcal/mol with a preexponential of 10^{13} s^{-1}, in reasonable agreement with the kinetics of the second step in the production of gaseous IBO from Cl^{t}BuO at low coverages. We therefore conclude that the IBO peak at 235 K is the result of a process involving two kinetically significant steps: C−Cl scission that deposits Cl atoms and IBO molecules on the Ag(110) surface, followed by desorption of molecularly adsorbed IBO.

Recall that the stoichiometric reaction of Cl^{t}BuOH with 0.1 ML of oxygen atoms yields 0.2 ML of Cl^{t}BuO(ad). If C−Cl scission of these species proceeded to completion without product desorption, the surface would contain at least 0.4 ML of adsorbates (plus any OH or H_2O from the initial titration reaction whose removal was not complete below 250 K). Given the bulkiness of adsorbates such as IBO and Cl^{t}BuO, such a surface would be rather crowded. Even for an initial O atom coverage of 0.1 ML, as shown in Figure 1, the C−Cl scission process does not go to completion below 250 K. Instead, a significant portion of the reaction is delayed, giving rise to a TPD peak at 315 K. For higher initial coverages, the low-temperature reaction channel is nearly completely suppressed; the rise of the surface Cl signal in TPXPS does not even begin below 250 K (Figure 6), and the 315 K IBO desorption peak is dominant.

The same procedure as above was followed to analyze the TPXPS and TPD spectra for the reaction of Cl^{t}BuOH with the higher oxygen atom coverage (0.3 ML initially) on the surface. The best simulation of the TPXPS results for the rise of the atomic chlorine signal was obtained for an activation barrier of

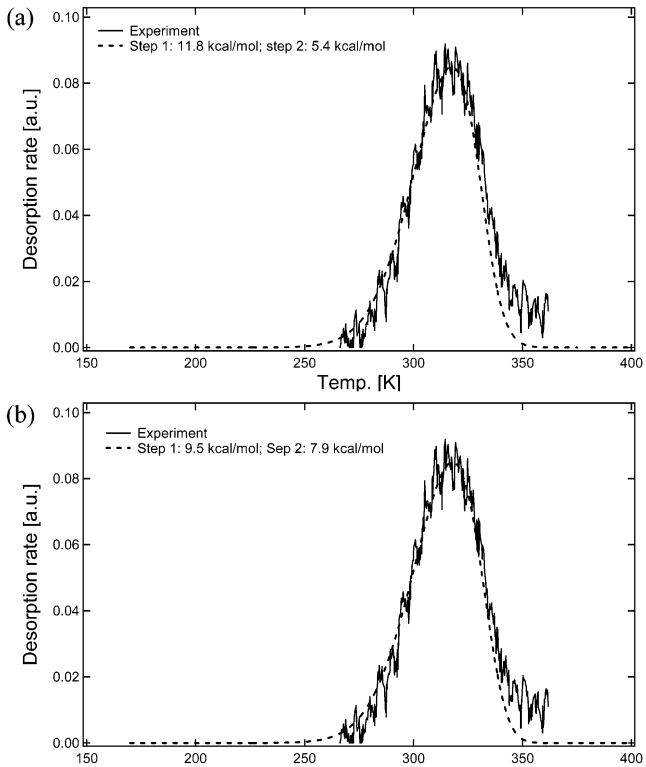

Figure 10. Match of predicted and measured TPD results at high oxygen atom coverage (0.3 ML) for a two-step model, using kinetic parameters for the first step derived from TPXPS.

11.8 kcal/mol and a preexponential factor of 4.7×10^7 s^{-1}, as shown in Figure 9a. However, as on the lower coverage surface, reasonable fits could be obtained with a range of activation energies between 9.8 and 12.8 kcal/mol with corresponding preexponentials ranging from 1.5×10^6 to 2.7×10^8 s^{-1}. Thus, the activation barriers for the C−Cl scission channels observed may not be very different; however, the preexponential factors required to fit the TPXPS results in Figures 7 and 9 must differ by 2 orders of magnitude if one uses a common activation energy. The low preexponentials obtained on the high-coverage surface suggest that the rate of C−Cl scission may be influenced by other factors, for example, the availability of surface sites on which to deposit the Cl atoms released by this reaction.

As shown above, following C−Cl scission via the low-temperature channel at low coverages, there is a delay in the appearance of the IBO product in the gas phase. This is also the case for the high-temperature channel at higher coverages. As shown in Figure 9, the TPD peak at 315 K cannot be produced by a single, first-order reaction with rate parameters obtained from the TPXPS experiments. As for the low-temperature channel on the low-coverage surface, a second step accounting for the release of IBO into the gas phase by desorption or reaction of a dechlorinated surface intermediate must be included to adequately reproduce the TPD results. Figure 10a illustrates the best fit to the TPD results obtained by fixing the rate parameters for C−Cl scission (11.8 kcal/mol, 4.7×10^7 s^{-1}) and varying the parameters for the second step. The values obtained for the second step were Ea = 5.4 kcal/mol for a preexponential factor of 720 s^{-1}. If the activation barrier assumed for C−Cl scission was decreased by ca. 2 kcal/mol, the best fit to the TPD results was obtained by increasing the activation barrier for the second step by roughly the same amount (with adjustment of the preexponentials). Figure 10b illustrates the fit to the TPD data for Ea_1 = 9.5 kcal/mol and Ea_2 = 7.9 kcal/mol; it is not significantly different from that in

Figure 10a for $Ea_1 = 11.8$ kcal/mol and $Ea_2 = 5.4$ kcal/mol. In either case, the activation energies for the second step are remarkably low for a process occurring above room temperature, and the apparent preexponentials are many orders of magnitude below "normal" values as well. As discussed in greater detail below, these low values may reflect a lack of available surface sites on this very crowded surface. A key point, however, is that Figures 7b and 9b clearly demonstrate that Cl^{t}BuO decomposition does *not* occur by an elementary S_N2 process that releases IBO directly into the gas phase. The combination of TPXPS and TPD results shows that C−Cl scission deposits organic intermediates or products on the surface and that the appearance of these products in the gas phase lags the appearance of atomic chlorine on the surface.

4. Discussion

The high spatial and temporal resolution of the synchrotron-based XPS experiments conveys at least three important advantages in this study of complex surface reaction processes. First, as is immediately apparent from Figure 2, it provides considerably better energy resolution, and therefore chemical resolution, than laboratory-based systems. Although one can make an educated guess about the contributions of different chemical species to the spectra of mixed adlayers comprising organic and atomic chlorine species, synchrotron-based XPS permits quantitative resolution of these. Second, in the transient mode such as TPXPS, it permits one to track surface C−Cl bond scission processes directly that do not give rise to coincident gas-phase products. One can extract the kinetics of these processes from analysis and modeling of extent of reaction versus temperature, as shown above. Most importantly, the combination of TPXPS with TPD analysis of desorption products permits one to unravel surface reaction sequences involving transient surface species and to access elementary reaction processes involving such species. In the particular case of the chemistry of chloro-*tert*-butyl alcohol on oxygen-containing Ag(110) surfaces, these point to the crucial influence of surface or subsurface diffusion processes, as developed below.

As illustrated above, one can account for the kinetics of IBO production, whether at high or low coverages, by two kinetically significant steps. At low coverages, these steps are the C−Cl scission of Cl^{t}BuO intermediates, and the desorption of molecularly adsorbed IBO molecules. Whether the production of *adsorbed* IBO from Cl^{t}BuO(ad) is an S_N2 (concerted) or S_N1 (sequential) process, one cannot say. The somewhat low preexponential factor obtained for C−Cl scission ($<10^{11}$ s^{-1}) at low coverages is indicative of a large negative value for $\Delta S^{\ddagger}$ for this step, consistent with a complex rearrangement/cyclization. However, the even lower preexponentials observed for processes on the high-coverage surface suggest that some caution is in order. Clearly, the kinetics of the second step in the sequence leading to gaseous IBO from the low-coverage surface are consistent with those observed for desorption of molecularly adsorbed epoxides on Ag(110), and this step is therefore assigned to desorption of adsorbed product IBO molecules.

While the production of IBO via the higher-temperature channel at higher coverages can also be explained by a two-step sequence, the values of the rate parameters obtained are more challenging to explain. The value of $\Delta G^{\ddagger}$ for the C−Cl scission step on the high-coverage surface is approximately 2.8 kcal/mol greater than on the low-coverage surface, if one compares the "best fit" parameters in each case. While the data are not sufficient to apportion this difference between energies and entropies of activation, it is plausible to ascribe this higher barrier to greater steric hindrance to reaction on the high-coverage surface. As noted above, starting with 0.3 monolayers of oxygen atoms should yield 0.6 monolayers of bulky Cl^{t}BuO intermediates on the surface. C−Cl scission would produce 1.2 monolayers of fragments on the surface, if the products of this process were retained on the surface throughout (which they are not). It is not surprising, therefore, that this process is more highly activated at high-surface coverages than at low.

Another possibility is that the local structure of the silver surface may be different in the high-coverage case. At high oxygen coverages (approaching 0.5 monolayers), the Ag(110) surface has been shown to undergo an added row reconstruction which exhibits (2×1) periodicity in LEED.[32] STM evidence for added row reconstructions at lower oxygen coverages corresponding to (3×1) and (4×1) LEED patterns has also been reported.[33] If the added row structure (or some variant of it) is preserved upon titration of surface oxygen atoms with alcohols, then the alkoxide intermediates synthesized on high initial oxygen coverage surfaces will find themselves in a different local environment than those synthesized on low coverage, nonreconstructed surfaces. The 2.8 kcal/mol difference in activation barriers for C−Cl scission of Cl^{t}BuO(ad) would not be unreasonable in such a case, especially if one considers that the Cl atoms deposited on the surface are larger and interact more strongly with the silver surface than, for example, the hydrogen atoms released by β-hydride eliminations typical of primary and secondary alkoxides. C−Cl scission would thus be expected to be more sensitive to surface geometric structure than would C−H scission.

Much more surprising are the incredibly low preexponential factors (of order 10^3 to 10^5 s^{-1}) for the second step in the evolution of IBO from Cl^{t}BuO decomposition at high coverages. The low activation energies (5−8 kcal/mol) and low preexponentials immediately suggest that the controlling process is diffusion, rather than chemical reaction. A first-order preexponential of 10^5 s^{-1} corresponds to a preexponential factor for a surface diffusion coefficient of 10^{-15} m^2/s, if one assumes that the characteristic length scale is about one lattice constant.[34] Seebauer and Jung have recently provided a comprehensive compilation of surface diffusion coefficients, primarily for atomic species. While typical values for the preexponentials for intrinsic diffusion (D°) on metal surfaces are 10^{-7} m^2/s, the reported values span 12 orders of magnitude about this median.[34] Preexponentials for diffusion on "corrugated" surfaces, such as FCC (110) surfaces, tend to appear on the lower end of the distribution. Moreover, low preexponentials for diffusion are typically associated with low activation energies for diffusion (i.e., there is a "compensation effect," as is often observed for reaction rate constants). The activation energy obtained for the second step in IBO desorption from the high-coverage surface (5−8 kcal/mol) is also on the low side of the values compiled by Seebauer and Jung.[34]

If the second step in IBO production from Cl^{t}BuO at high coverage is limited by diffusion, what is diffusing and how does it influence the reaction rate? In principle, the diffusing species could be any adsorbed product derived from C−Cl scission of the Cl^{t}BuO(ad) intermediate. Organic species might include a radical intermediate or an oxametallacycle formed by the C−Cl scission, or molecular IBO. It seems improbable that a molecular product would need to diffuse to some other site before desorbing. However, given the multidentate coordination of oxametallacycles on silver,[5,10] it might be necessary for the initial product of Cl^{t}BuO C−Cl scission to access more open sites on

the surface for cyclization to proceed. This might occur either by diffusion of the organic moieties on the high-coverage surface or diffusion of the deposited chlorine atoms away from the site of their initial deposition (and away from the organic fragment with which each was initially associated).

The problem with either scenario is that, for most of the course of reaction, surface diffusion processes at best would simply rearrange species on a rather densely covered surface. We favor diffusion of chlorine atoms as the controlling process, because these can access another channel that results in opening of surface sites—they can diffuse *into* the surface. Bowker and Waugh[27,35] have shown that chlorine dissolution into the Ag(110) and (111) surfaces occurs at 300 K in UHV, precisely the temperature range covered by Cl^{t}BuO decomposition and IBO desorption in the present study. The TPXPS results provide further corroboration. Figure 6 shows a slowly declining signal for atomic chlorine on the surface above 300−350 K. Since no chlorine desorption occurs at this temperature, diminution of the Cl2p signal by diffusion of chlorine atoms into subsurface layers is the most credible explanation. The deviation of the TPXPS results from the kinetic model for C−Cl scission evident in Figure 9a above ca. 300 K is also consistent with the loss of Cl atoms from the surface to the subsurface in Cl^{t}BuO decomposition. The fact that the relevant diffusion process is a solid-state one may explain the observation that the diffusion coefficient is on the low side of expected values for surface diffusion, as discussed above.

We conclude, therefore, that while C−Cl scission of Cl^{t}BuO can proceed on densely covered surfaces (albeit with a higher activation barrier than on more sparsely populated surfaces), completion of the ring closure reaction to produce IBO is limited by the availability of surface sites capable of coordinating multidentate oxametallacycle intermediates. Diffusion of Cl atoms into the silver surface creates such sites over the same temperature interval as the C−Cl scission reaction. Whether the limitation is to formation of the oxametallacycle or its ring closure to liberate IBO, this scheme implies that the formation of IBO from Cl^{t}BuO at high coverages is an S_N1 process. The combination of TPXPS and TPD results provides clear evidence for distinct C−Cl scission and IBO production processes. In the low-temperature/low-coverage channel, the latter process may simply be IBO desorption; in the higher-temperature/high-coverage channel, IBO formation from a dechlorinated surface intermediate is a distinguishable process limited by diffusion of Cl atoms into the silver surface.

5. Conclusions

Temperature-programmed X-ray photoelectron spectroscopy (TPXPS) and temperature-programmed desorption (TPD) techniques have been used to determine whether the surface chlorohydrin reaction of Cl-*t*-BuOH on Ag(110) follows an S_N1 or S_N2 mechanism. At low initial coverages, surface Cl^{t}BuO species, formed by reaction of the alcohol with surface oxygen atoms, dechlorinate between 200 and 300 K. The appearance of IBO in the gas phase lags the rate of deposition of chlorine atoms on the surface (tracked by TPXPS), and the lag can be accounted for by a two-step model incorporating the desorption kinetics of the molecular IBO product. At high coverages, the onset of the C−Cl scission reaction is increased by 50 K, but the production of IBO still lags Cl deposition. In this case, the formation of IBO is influenced by the rate of diffusion of Cl atoms into the silver, which liberates surface sites for cyclization of a dechlorinated surface intermediate to form IBO. This implies that the formation of IBO from Cl^{t}BuO on the Ag(110) surface proceeds by an S_N1 pathway. The combination of transient TPXPS and TPD experiments was essential to detect and to quantify differences in the rates of surface reaction processes versus the appearance of gas-phase products and to determine the contributions of surface reaction and diffusion phenomena to these.

Acknowledgment. This study was supported by the Seed Catalysis Project funded by the U.S. Department of Energy, Basic Energy Sciences under Contract No. DE-AC02-98-CH10886. H. Piao acknowledges the financial support by Natural Sciences and Engineering Research Council of Canada. D.R.M. was supported under contract DE-AC05-00OR22725 with Oak Ridge National Laboratory, managed and operated by UT-Battelle, LLC. S. Hulbert, C.-C. Kao, and Q.-L. Dong at the National Synchrotron Light Source at Brookhaven National Laboratory are gratefully acknowledged for their technical support. We also thank J. A. Rodriguez, G. Liu, and P. Liu for useful discussions.

References and Notes

(1) Jones, G. S.; Barteau, M. A. *J. Vac. Sci. Technol. A* **1997**, *15*, 1667.
(2) Jones, G. S.; Mavrikakis, M.; Barteau, M. A.; Vohs, J. M. *J. Am. Chem. Soc.* **1998**, *120*, 3196.
(3) Mavrikakis, M.; Doren, D. J.; Barteau, M. A. *J. Phys. Chem. B* **1998**, *102*, 394.
(4) Medlin, J. W.; Mavrikakis, M.; Barteau, M. A. *J. Phys. Chem. B* **1999**, *103*, 11169.
(5) Medlin, J. W.; Barteau, M. A.; Vohs, J. M. *J. Mol. Catal. A* **2000**, *163*, 129.
(6) Ihm, H.; Medlin, J. W.; Barteau, M. A.; White, J. M. *Langmuir* **2001**, *17*, 798.
(7) Medlin, J. W.; Sherrill, A. B.; Chen, J. G.; Barteau, M. A. *J. Phys. Chem. B* **2001**, *105*, 3769.
(8) Medlin, J. W.; Barteau, M. A. *Surf. Sci.* **2002**, *506*, 105.
(9) Medlin, J. W.; Barteau, M. A. *J. Phys. Chem. B* **2001**, *105*, 10054.
(10) Linic, S.; Barteau, M. A. *J. Am. Chem. Soc.* **2002**, *124*, 310.
(11) Linic, S.; Medlin, J. W.; Barteau, M. A. *Langmuir* **2002**, *18*, 5197.
(12) Saravanan, C.; Salazar, M. R.; Kress, J. D.; Redondo, A. *J. Phys. Chem. B* **2000**, *104*, 8685.
(13) Wu, G.; Stacchiola, D.; Kaltchev, M.; Tysoe, W. T. *Surf. Sci.* **2000**, *463*, 81.
(14) Stacchiola, D.; Wu, G.; Kaltchev, M.; Tysoe, W. T. *Surf. Sci.* **2001**, *486*, 9.
(15) Stacchiola, D.; Wu, G.; Kaltchev, M.; Tysoe, W. T. *J. Mol. Catal. A-Chem.* **2001**, *167*, 13.
(16) Yan, X. M.; Kim, C.; White, J. M. *J. Phys. Chem. B* **2001**, *105*, 3587.
(17) Carey, F. A. *Organic Chemistry*, 2nd ed.; McGraw-Hill: New York, 1992.
(18) Brainard, R. L.; Madix, R. J. *J. Am. Chem. Soc.* **1989**, *111*, 3826.
(19) Baraldi, A.; Comelli, G.; Lizzit, S.; Kiskinova, M.; Paolucci, G. *Surf. Sci. Rep.* **2003**, *49*, 169.
(20) Dai, Q.; Gellman, A. J. *J. Am. Chem. Soc.* **1993**, *115*, 714.
(21) Wachs, I. E.; Madix, R. J. *Appl. Surf. Sci.* **1978**, *1*, 303.
(22) Dai, Q.; Gellman, A. *Surf. Sci.* **1991**, *257*, 103.
(23) Kim, K. S.; Barteau, M. A. *J. Catal.* **1990**, *125*, 353.
(24) Kim, K. S.; Barteau, M. A. *Langmuir* **1990**, *6*, 1485.
(25) Rufael, T. S.; Huntley, D. R.; Mullins, D. R.; Gland, J. L. *J. Phys. Chem.* **1995**, *99*, 11472.
(26) White, G.; Woll, Ch. *J. Chem. Phys.* **1995**, *103*, 5860.
(27) Bowker, M.; Waugh, K. C. *Surf. Sci.* **1985**, *155*, 1.
(28) Gelius, U.; Hedén, P. F.; Hedman, J.; Lindberg, B. J.; Manne, R.; Nordberg, R.; Nordling, C.; Siegbahn, K. *Phys. Scr.* **1970**, *2*, 70.
(29) Barr, T. L.; Yin, M. P. *J. Vac. Sci. Technol. A* **1992**, *10*, 2788.
(30) Barr, T. L. *Modern ESCA*; CRC Press: Boca Raton, FL, 1994.
(31) Barr, T. L. In *Practical Surface Analysis*, 2nd ed.; Briggs, D., Seah, M. P., Eds.; Wiley: Chichester, U.K., 1990.
(32) Guo, X.-C.; Madix, R. J. *J. Phys. Chem. B* **2003**, *107*, 3105.
(33) Guo, X.-C.; Madix, R. J. *J. Phys. Chem. B* **2001**, *105*, 3878.
(34) Seebauer, E. G.; Jung, M. Y. L. In *Landolt-Börnstein Numerical Data and Functional Relationships: Adsorbed Layers on Surfaces*; Bonzel, H. P., Ed.; Springer-Verlag: New York, 2001; Vol. III/42A.
(35) Bowker, M.; Waugh, K. C. *Surf. Sci.* **1983**, *134*, 639.